A&A, 682, L20 (2024)
https://doi.org/10.1051/0004-6361/202449359

Astronomy & Astrophysics

Letter to the Editor

Observations of the new meteor shower from comet 46P/Wirtanen

D. Vida[1,2], J. M. Scott[3], A. Egal[4,1,5], J. Vaubaillon[4], Q.-Z. Ye[6,7], D. Rollinson[8], M. Sato[9], and D. E. Moser[10]

[1] Department of Physics and Astronomy, University of Western Ontario, London, Ontario N6A 3K7, Canada
e-mail: dvida@uwo.ca
[2] Institute for Earth and Space Exploration, University of Western Ontario, London, Ontario N6A 5B8, Canada
[3] Department of Geology, University of Otago, Dunedin, New Zealand
[4] Planétarium de Montréal, Espace pour la Vie, 4801 av. Pierre-de Coubertin, Montréal, Québec, Canada
[5] IMCCE, Observatoire de Paris – PSL, 77 av. Denfert-Rochereau, 75014 Paris, France
[6] Department of Astronomy, University of Maryland, College Park, MD 20742, USA
[7] Center for Space Physics, Boston University, Boston, MA 02215, USA
[8] Perth Observatory Volunteer Group, Bickley, Western Australia
[9] National Astronomical Observatory of Japan, Tokyo, Japan
[10] NASA Meteoroid Environment Office, Marshall Space Flight Center, Huntsville, AL 35812, USA

Received 26 January 2024 / Accepted 6 February 2024

ABSTRACT

Context. A new meteor shower λ-Sculptorids produced by the comet 46P/Wirtanen was forecast for December 12, 2023. The predicted activity was highly uncertain, but generally considered to be low. Observations in Australia, New Zealand, and Oceania were solicited to help constrain the size distribution of meteoroids in the shower.

Aims. This work aims to characterize the new meteor shower, by comparing the observed and predicted radiants and orbits, and to provide a calibration for future predictions.

Methods. Global Meteor Network video cameras were used to observe the meteor shower. Multi-station observations were used to compute trajectories and orbits, while single-station observations were used to measure the flux profile.

Results. A total of 23 λ-Sculptorid orbits have been measured. The shower peaked at a zenithal hourly rate (ZHR) of $0.65^{+0.24}_{-0.20}$ meteors per hour at $\lambda_\odot = 259.988° \pm 0.042°$. Due to the low in-atmosphere speed of 15 km s^{-1}, the mean mass of observed meteoroids was 0.5 g (~10 mm diameter), an order of magnitude higher than predicted. The dynamical simulations of the meteoroid stream can only produce such large meteoroids arriving at Earth in 2023 with correct radiants when a very low meteoroid density of ~100 kg m^{-3} is assumed. However, this assumption cannot reproduce the activity profile. It may be reproduced by considering higher density meteoroids in a larger ecliptic plane-crossing time window (ΔT = 20 days) and trails ejected prior to 1908, but then the observed radiant structure is not reproduced.

Key words. comets: individual: 46P/Wirtanen – meteorites, meteors, meteoroids

1. Introduction

Before launch delays, the comet 46P/Wirtanen was initially selected as the primary target for the Rosetta mission due to its favourable orbit and interesting characteristics (Rickman & Jorda 1998). At the time, the comet was interesting as it had one of the largest nongravitational accelerations of any comet that had undergone a recent orbital perturbation (i.e., close approaches to Jupiter in 1972 and 1984), indicating a high fraction of actively outgassing area (Schulz & Schwehm 1999; Groussin & Lamy 2003). The comet had a very close approach to Earth in 2018, coming within 0.077 AU. Moulane et al. (2023) performed observations using TRAPPIST telescopes and found that the comet is "hyperactive", with 40% of its surface active and having the activity parameter $Af\rho(0)$ of 250 cm. In comparison, typical Jupiter-family comets have active areas between 5–10% (A'Hearn et al. 1995). In a study relevant to this work, Coulson et al. (2020) found the possible presence of mm-sized dust in the 46P's coma, meaning that they could be detected optically upon entering the atmosphere.

The comet's orbit has a very low minimum orbit intersection distance (MOID) to Earth of only 0.071 AU, which made it a target of investigation as a potential meteor shower parent body (Ye & Jenniskens 2022). Maslov & Muzyko (2017) predicted possible low-activity outbursts in 2017 and 2019 with a zenithal hourly rate (ZHR) not exceeding 5–10 meteors per hour. No positive confirmations of the outbursts have been made in those years. Vaubaillon et al. (2023) performed a separate set of simulations using five different methods that mostly differ in terms of the conditions of meteoroid ejection from the comet and in the modeling of non-gravitational forces during orbital integration. The dynamical models by the co-authors are referred to in this paper by their initials: AE (Egal et al. 2019), JV (Vaubaillon et al. 2005a,b), QY (Ye et al. 2016), MS (Watanabe et al. 2005), and DM (Moser & Cooke 2004, 2008)). All models roughly agreed and found no significant encounters of ejected particles with the Earth in the past, except in 2007 and 2018 with the 1974 trail. A search on Canadian Meteor Orbit Radar (CMOR) data, which spans over two decades (Brown et al. 2010) was performed for these years, as well as

the years predicted by Maslov & Muzyko (2017); however, no conclusive detections have been found. However, due to the slow speed of meteoroids, which severely impacts the ionization efficiency and the meteor shower geocentric radiants being under the horizon, only a fraction of the largest meteoroids could even be theoretically detectable due to zenithal attraction (Gural 2001).

For 2023, all five models of Vaubaillon et al. (2023) predict an encounter with the 1974 trail ranging in time between December 12 08:23 UT and 20:06 UT. In addition, the AE model predicts encounters with trails ejected between 1900 and 1945 a bit later, between December 12 at 17:05 UT and December 13 at 06:26 UT. Due to a lack of calibration on observations, only the upper limit on the ZHR has been provided, estimated not to exceed ten meteors per hour on average. The predicted distribution of geocentric radiants on the sky was roughly diagonal and spanned about 15°, from approximately RA = 10°, Dec = −45° to RA = 6°, Dec = −33°. The large extent of the radiant locations was due to the uncertainty in encounter parameters and included all meteoroids within 0.05 AU from Earth. However, meteoroids that were predicted to come the closest, within 0.001 AU, were all concentrated in a tight 1° radius around RA = 7.75°, Dec = −39°. The radiant at the nominal peak time on December 12 at 10:15 UT was predicted to be in the zenith just off the southwestern tip of Australia, located at the edge of the Earth's terminator. The best locations for optical observations were thus in Australia, New Zealand, and the rest of the Southwest Pacific. The meteor shower was initially referred to as the "Wirtanenids", but Vaubaillon et al. (2023) suggested a new name for the shower, λ-Sculptorids, which has been accepted by the International Astronomical Union (IAU) for the name of the shower and this term is used herein to refer to the shower. The provisional designation for the shower by the IAU Meteor Data Center is M2023-Y1.

In this work, we report the first conclusive observations of meteors produced by dust ejected from comet 46P/Wirtanen. In Sect. 2, we describe the hardware and methods used by the Global Meteor Network. In Sect. 3, we present the results of observations and the comparison to predictions.

2. Methods

The Global Meteor Network (GMN[1]) is a professional-amateur consortium that currently operates over 1000 video meteor cameras globally (Vida et al. 2021). The network has over 200 cameras in the Southwest Pacific region, mostly operated by Fireballs Aotearoa[2] in New Zealand, Perth Observatory in Western Australia[3], and a number of independent citizen scientists. An average GMN camera system consists of a commercial off-the-shelf (COTS) video camera with a Sony IMX291 sensor, coupled to a 3.6 mm $f/0.95$ lens and a Raspberry Pi single-board computer for data capture and processing. The optical setup achieves similar performance to human vision, with a field of view (FoV) of 88° × 48°, a frame rate of 25 frames per second and a stellar limiting magnitude in average sky conditions of +6.0 (Vida et al. 2021). In addition, a pair of six-camera stations in Western Australia (Pemberton and Toodyay) were operated with 6 mm lenses with a FOV of 53° × 30° and a stellar limiting magnitude of +6.5.

Individual cameras report to a central server that performs meteor trajectory correlation and meteor shower flux computation. Multi-station trajectories and orbits are computed using the method described in Vida et al. (2020b), which provides realistic uncertainties of orbital parameters by using Monte Carlo error estimation. Meteor shower flux is computed from single-station observations using the method described in Vida et al. (2022). The total observed atmospheric area at the height of the meteor shower is estimated by applying bias corrections, which take into account the theoretical radiant elevation, meteor angular velocity, and measured camera sensitivity and vignetting. An algorithm is employed to determine periods of clear skies by matching observed stars to their computed positions and numbers assuming modeled observational biases. The method produces a meteor activity profile in units of meteoroids per 1000 square kilometres at a given mass limit, together with a profile of observation efficiency, which informs the completeness of the results (e.g., a peak might be missing in the activity profile if all cameras were clouded out at that time). In practice, for any new meteor shower, meteor trajectories are computed first and the radiant location, radiant drift, radiant dispersion, meteor velocity, average meteor height, and meteoroid mass distribution index are manually measured. These data are then put in the flux algorithm.

3. Observation results and comparison to simulations

During the time of the predicted λ-Sculptorid activity, most of New Zealand was under cloud cover, with only a handful of cameras of Fireballs Aotearoa having clear skies the whole night. The weather in Australia was excellent, with most cameras observing uninterrupted the whole night. Qualitatively speaking, the observed activity was very low, with each camera observing on the order of one λ-Sculptorid meteor during the whole night.

3.1. Trajectories and orbits

A total of 23 λ-Sculptorid meteoroid trajectories and orbits were computed, the details of which are given in Table A.1. All were observed in either New Zealand or Australia, except for one each from South Korea and Bulgaria where the radiant was under the horizon but the trajectories were bent by Earth's gravity enabled by the extremely low speed of the shower (i.e., zenithal attraction). The observed median geocentric radiant is $\alpha_g = 6.89°$, $\delta_g = -38.89°$ in equatorial and $\lambda_g - \lambda_\odot = 88.10°, \beta_g = -38.19°$ in Sun-centered ecliptic coordinates. The radiant dispersion, measured as the median angular separation from the median radiant (Moorhead et al. 2021), is 0.96°. The median radiant measurement error is 0.52°, meaning that the true physical radiant dispersion has been resolved. The median observed geocentric velocity is $10.00 \pm 0.25\,\mathrm{km\,s^{-1}}$.

Figure 1 shows the comparison between model radiants and the observed GMN and CMOR radiants. The observed GMN radiant locations generally match well with the models. The mean observed geocentric declination matches almost exactly, with some models predicting it to be at the observed −38.8°, while the rest are all between −38.0° and −40.4° for the 1974 trail. However, there is a ∼1° shift in right ascension from the mean model radiant locations. In terms of the spread, the AE model radiants extend about 8° along the declination, while

[1] GMN website: https://globalmeteornetwork.org/ (accessed Jan. 8, 2024).
[2] Fireballs Aotearoa: https://fireballs.nz/ (accessed Dec. 25, 2023).
[3] Perth Observatory: https://www.perthobservatory.com.au/ (accessed Dec. 25, 2023).

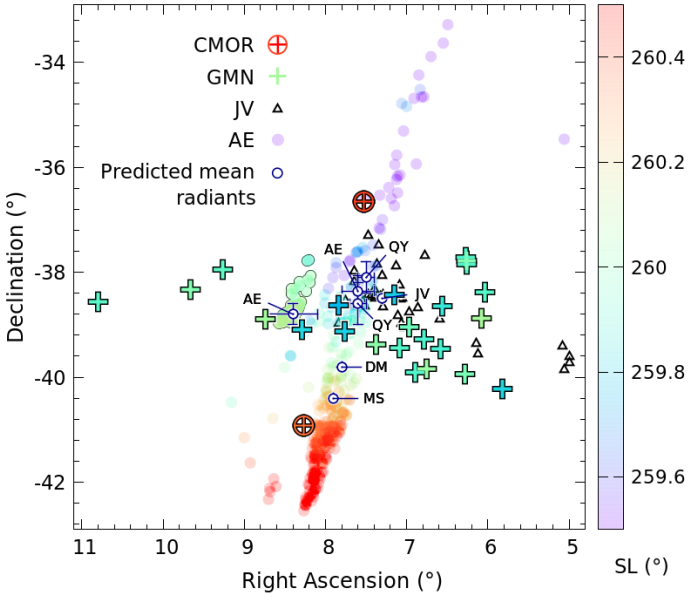

Fig. 1. Comparison between the geocentric radiants measured by GMN (crosses) and CMOR (circled crosses) and the various theoretical radiants proposed by Vaubaillon et al. (2023). The models are marked by the initials of individual co-authors. The coloured circles are radiants predicted by AE, based on the Egal et al. (2019) model, with mm-sized particles having a dark edge (to the left of the smaller particles). Triangles are model radiants predicted by JV using the Vaubaillon et al. (2005a) model. The radiants observed by the GMN are shown as crosses. The error bars are not plotted for better readability, but the average radiant measurement error is ~0.5°.

the JV radiants extend ~2° along the right ascension, matching the GMN video observations best. All models predicted a mean encounter geocentric velocity in the range between 9.8 and 10.3 km s^{-1}, which perfectly matches the observed value of 10.00 ± 0.25 km s^{-1}.

In addition to GMN, CMOR observed a total of four λ-Sculptorid meteors, despite being located in Canada. Two had large measurement uncertainties due to the extremely low speed. The other two have been observed well and presented in the figure. The improved atmospheric deceleration correction for CMOR (Froncisz et al. 2020) enabled accurate measurement of the pre-atmospheric speed of these slow meteors. The electron line densities for the two meteors are around 10^{14} e m^{-1}, translating to a peak meteor magnitude of about +5.5 and 3–5 mm diameter particles (Weryk & Brown 2013). To confirm the validity of the detection, a period of 20 days before the shower was investigated for additional detections, and not a single radiant was observed by CMOR within a 20° radius from the shower during that time. The two radiants (Fig. 1) were located exactly on the elongated radiant spread modeled by AE, matching that model best.

For reference, the mean orbital parameters using GMN data have been computed using the method of Jopek et al. (2006) and are given in Table 1 where they are compared to the mean of simulated orbits (JV), and the orbit of the comet 46P/Wirtanen at epochs in 2018 (latest orbit) and the time of meteoroid ejection in 1974. Compared to the comet, both the observed and simulated meteoroids have a smaller orbit, with the perihelion just inside the Earth's orbit. The mean observed and simulated orbits compare well and are well within the scatter in the orbital parameters for both (see Table A.1).

3.2. Physical properties

The shower meteors exhibited median begin and end heights of 90.1 ± 1.2 km and 78.2 ± 2.9 km, respectively. The median meteor peak height is 84.2 ± 2.5 km, translating into an F parameter of 0.54 ± 0.13. The observed absolute peak magnitudes ranged from the faintest meteor at +2.40 to the brightest at −0.45. The photometric masses were computed on integrated light curves using a fixed luminous efficiency of τ = 0.7% (Vida et al. 2018). The observed meteoroids had masses between 0.15–4.12 g, with a median mass of 0.47 g. Using a bulk density of 500 kg m^{-3} (Ceplecha et al. 1998), these masses correspond to diameters between 8–25 mm, and the median value of 12 mm.

We computed the Ceplecha (1958) K_B parameter to characterize the physical composition. Cordonnier et al. (2024) calibrated the parameter on GMN data and found that a value of −0.1 needs to be subtracted from the original definition, a correction that we also applied. The shower had a mean K_B of 6.972 ± 0.096, putting the meteors into group C1, defined as regular cometary material from short-period comets (Ceplecha 1988). This result is consistent with the comet's origin and orbit, making the meteoroids similar to the Taurids, for instance. A similar value of K_B has also been observed for the 2022 outburst of the τ-Herculids (Egal et al. 2023). That outburst was caused by similarly-aged meteoroids, ejected in 1995. Both comets were on a similar orbit with a $q \approx 1$ and the measured K_B for the τ-Herculids is 6.9 ± 0.2 (Koten et al. 2023). This is in contrast to the Draconids, which are also young (Egal et al. 2019), and have a parent body on a similar orbit, but are much more fragile, classified as group D (Koten et al. 2007). This indicates the physical structural strength of meteoroids is not only a function of age, but is inherent to the specificity of the material present in the parent comet.

3.3. Activity profile

Due to the small number of observed meteors, the population index has been difficult to measure. Using the method of Vida et al. (2020a), we found a mass index of $s = 2.25^{+1.5}_{-0.52}$ and a population index of $r = 3.23^{+3.03}_{-0.85}$. The errors are large due to the small sample size, making choosing a single nominal value difficult. We erred on the side of caution, choosing values of $s = 2.2$ and $r = 3.0$ which have been traditionally considered in the literature as values appropriate for showers rich in small particles (Rendtel 2004), as indicated from observations of 46P (Kareta et al. 2023; Vaubaillon et al. 2023). The chosen value is well within the uncertainty.

Figure B.1 in the appendix shows the observed flux profile of the λ-Sculptorids and the data is given in Table A.2. The shower peaked at solar longitude $\lambda_\odot$ = 259.988° ± 0.042° (2023-12-12 15:04 UTC ± 1 h). The peak flux was $0.179^{+0.073}_{-0.057}$ meteoroids per 1000 km^2 per hour at a limiting magnitude of +5.42 and limiting mass of 1.5×10^{-5} kg. Translated to zenithal hourly rate (ZHR), the peak activity was $0.65^{+0.24}_{-0.20}$ meteors per hour. The observed activity period spanned solar longitudes between 259.735° and 260.318708° (09:06 UTC to 22:53 UTC), with the threshold ZHR of around 0.1 meteors per hour. The network had excellent observational coverage throughout the activity period and had no coverage gaps. The minimum time-area product (TAP) per bin is set to 15 000 km^2 h and the minimum number of meteors per bin is set to 10, allowing for a temporal resolution of about 1 h. The bin duration was limited by the number of meteors in each bin and not the TAP, showing the scarcity of observed meteors.

Table 1. Mean orbital elements of the observed λ-Sculptorids compared to the mean orbital elements of the simulated particles encountering the Earth in 2023 (JV model) and the comet 46P/Wirtanen.

Parameter	λ-Sculptorids	Simulated	46P/Wirtanen	46P/Wirtanen	
Epoch	J2000	J2000	2458465.5	2442240.5	
Date	2023-12-12	2023-12-12	2018-12-13	1974-07-12	
a	2.891	3.029	3.092662	3.255261	AU
q	0.984566	0.980229	1.05535538	1.255701	AU
e	0.65946	0.676399	0.6587550	0.614255	
i	9.200	8.364	11.747548	12.2672	deg
Ω	79.925	79.432	82.157634	84.2087	deg
ω	359.915	0.284	356.341072	351.8580	deg

Notes. JPL Horizons: https://ssd.jpl.nasa.gov/tools/sbdb_lookup.html#/?sstr=46P (accessed Dec. 25, 2023).

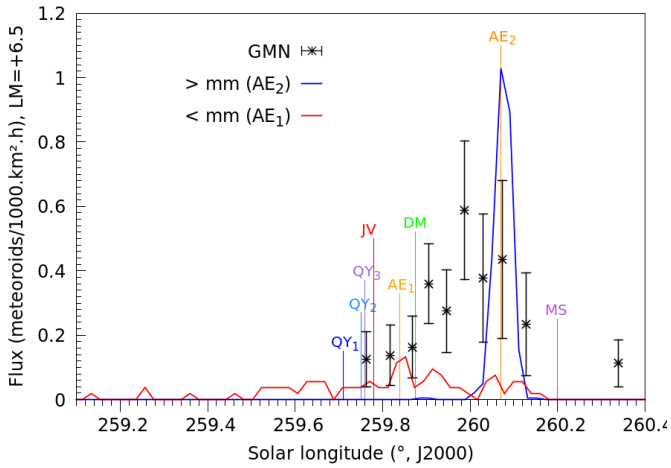

Fig. 2. Comparison between the observed flux profile of the λ-Sculptorids with the predictions of Vaubaillon et al. (2023). Coloured lines indicate the maximum activity time predicted by the different models presented in Table 2 of Vaubaillon et al. (2023), and marked by the initials of the co-authors. The solid lines illustrate the modeled activity predicted by AE for particles with sizes above (blue) or below (red) one millimetre, with nodal-crossing locations closer than 0.02 AU from the Earth's orbit at the time of the shower (AE_1 model). The black symbols represent the flux measured by GMN at a limiting magnitude of +6.5.

Figure 2 shows the comparison between the predicted and observed activity profiles. Vaubaillon et al. (2023) found that different ejection conditions at the comet highly influence the shower's predicted time, which varied from 259.71° to 260.20° in solar longitude. In addition, the trails released by 46P display a complicated dynamical evolution that is typical of JFC meteoroid stream (Vaubaillon et al. 2004). This is particularly true for the 1974 trail, which suffered a close encounter with Jupiter in 1984 that significantly changed the meteoroids' orbital elements, causing the positions of the comet and the trail to reverse, putting the meteoroids in a leading position in front of the comet (see the comparison of the orbital elements before and after the encounter in Fig. B.2).

All models in Vaubaillon et al. (2023) predicted a meteor activity caused by the 1974 trail. However, only the smallest meteoroids (<1 mm) of the trail were found to approach the Earth in 2023, with masses below the detection limit of GMN cameras. This discrepancy can be resolved if models considered lower particle densities than the predicted values of 500–1000 kg m^{-3}. Additional simulations conducted by JV with a density of 100 kg m^{-3} show that massive particles from the 1974 trail are able to reach the Earth in 2023, with radiants and arrival times similar to those of Vaubaillon et al. (2023) and matching the observed radiant locations but not the peak time and activity profile. This low density is plausible as the shower's K_B parameter is similar to that of the τ-Herculids which also had a very low measured bulk density of 250 kg m^{-3} (Egal et al. 2023).

Additional investigations of the AE_1 simulations, motivated by the observational constraints, highlight the influence of the particles' selection criterion on the modeled activity profile. In the simulations, only particles crossing the ecliptic plane within a distance ΔX and time ΔT from the Earth are retained as potential impactors. For a standard $\Delta X < 0.02$ AU and $\Delta T \pm 7$ days, only particles from the 1974 trail and the 1900–1908+ trails produced detectable meteors (model AE_1 in Vaubaillon et al. (2023)), as shown in Fig. 2.

By increasing ΔT to 20 days, we find the modeled profile to be in better agreement with the observations (blue curve in Fig. 3). The temporal ΔT selection amounts to replacing each simulated particle p with a swarm of particles of identical orbits centred on p, which crosses the ecliptic plane at the nodal during a period of $2\Delta T$. Large ΔT values, representing a high uncertainty on the particles' position along the orbits, have been employed to successfully predict the return of past meteor showers (Jenniskens & Vaubaillon 2008; Egal et al. 2020).

With this less restrictive ΔT criterion, several trails ejected prior to 1908 are found to contribute to the shower's activity in 2023. The resulting activity profile reproduces well the timing and duration reported for the shower. In contrast, the modeled radiants remained similar to those presented in Fig. 1, and do not reproduce the observed spread in right ascension as well as the JV model. While additional observations could help assess the real contribution of trails ejected from the comet prior to 1974, no significant activity of the λ-Sculptorid is expected until 2045 in the AE_1 model.

4. Conclusions

We have presented the first observations of meteors from a new meteor shower λ-Sculptorids produced by the comet 46P/Wirtanen. The dynamical simulations by Vaubaillon et al. (2023) predicted that meteoroids from the 1974 trail encounter the Earth on December 12, 2023. The authors used several different methods and thus the exact predicted time of the peak varied between 08:23 UT and 20:06 UT.

A total of 23 multi-station meteors were observed by video meteor cameras of the Global Meteor Network for which trajectories were correlated, and a total of 172 from single-station

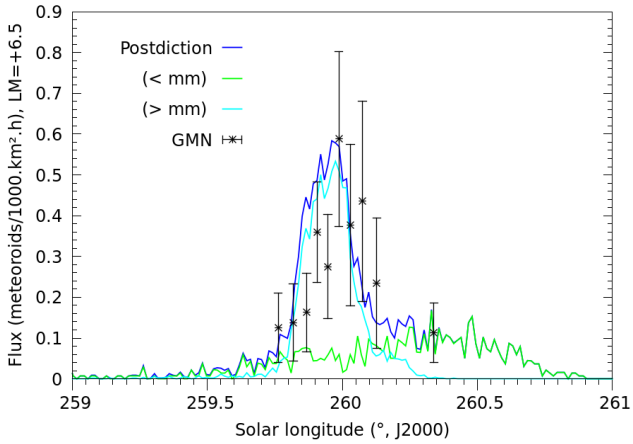

Fig. 3. Updated modeled activity (postdiction) of the λ-Sculptorid shower from the AE_1 simulation data set, for sub-mm (green) and mm-sized (cyan) particles. In Vaubaillon et al. (2023), only particles crossing the ecliptic plane closer than $\Delta r = 0.02$ AU and within $\Delta T \pm 7$ days from the Earth were retained in AE_1's simulation. By increasing the time selection criterion to 20 days, more mm-sized particles ejected from 46P prior to 1908 approached the Earth in 2023. The resulting activity profile (dark blue) is a better match to the observations when including the contribution of older trails.

λ-Sculptorids were used to estimate the flux. The activity peaked at 2023-12-12 15:04 UTC ± 1 h (solar longitude $\lambda_\odot$ = 259.988° ± 0.042°), while the total activity period (ZHR > 0.1) spanned between 09:06 UTC to 22:53 UTC (solar longitudes 259.735° and 260.318708°). The shower peaked at a ZHR of $0.65^{+0.24}_{-0.20}$ meteors per hour.

Due to the slow in-atmosphere speed of ~15 km s^{-1}, only the largest meteoroids were observed, with an average size of 10 mm. The measured value of K_B = 7.0 ± 0.1 indicates an ordinary short-period comet composition, similarly to the recent τ-Herculid outburst in 2022, which was produced by similarly young meteoroids ejected in 1995.

Trajectory, orbit, and activity level observations by the Global Meteor Network all matched the meteoroid stream dynamical simulations well overall. The radiants best match the predictions of JV for the 1974 trail if a very low bulk density of 100 kg m^{-3} is assumed. For higher densities, mm-sized and larger meteoroids do not reach the Earth in 2023 in all dynamical simulations. Alternatively, the observed activity profile and the mm-sizes can be achieved using older trails and if a larger threshold of time and range from the orbit is taken into account (i.e., AE model). However, this model reproduces the radiant structure less accurately than other models. The fundamental difficulty in reproducing the observations stems from the close encounter of the 1974 trail with Jupiter in 1984, which caused a significant shift in the orbital parameters. Any small model uncertainties are amplified by that event, setting a practical limit on the reproducibility of the observations. This makes the λ-Sculptorids an excellent data point for future model validation and improvement, as small differences in the model assumptions make large differences in the final result, helping to identify the best approach and model parameters.

Acknowledgements. The Global Meteor Network (GMN) data are released under the CC BY 4.0 license. The authors thank all GMN camera operators and contributors who are listed in Appendix C. We also thank Peter Brown for providing CMOR observations of the new shower. Q.Y. was supported by NASA grant 80NSSC21K0156, DV and AE were supported in part by the NASA Meteoroid Environment Office under cooperative agreement 80NSSC21M0073.

References

A'Hearn, M. F., Millis, R. C., Schleicher, D. G., Osip, D. J., & Birch, P. V. 1995, Icarus, 118, 223
Brown, P., Wong, D. K., Weryk, R. J., & Wiegert, P. 2010, Icarus, 207, 66
Ceplecha, Z. 1958, Bull. Astron. Inst. Czechoslovakia, 9, 154
Ceplecha, Z. 1988, Astron. Inst. Czechoslovakia Bull. (ISSN0004-6248), 39, 221
Ceplecha, Z., Borovička, J., Elford, W. G., et al. 1998, Spaces Sci. Rev, 84, 327
Cordonnier, L. E., Obenberger, K. S., Holmes, J. M., Taylor, G. B., & Vida, D. 2024, JGR: Space Phys., submitted
Coulson, I. M., Liu, F.-C., Cordiner, M. A., et al. 2020, AJ, 160, 182
Egal, A., Wiegert, P., Brown, P. G., et al. 2019, Icarus, 330, 123
Egal, A., Wiegert, P., Brown, P. G., Campbell-Brown, M., & Vida, D. 2020, A&A, 642, A120
Egal, A., Wiegert, P. A., Brown, P. G., & Vida, D. 2023, ApJ, 949, 96
Froncisz, M., Brown, P., & Weryk, R. J. 2020, Planet. Space Sci., 190, 104980
Groussin, O., & Lamy, P. 2003, A&A, 412, 879
Gural, P. 2001, WGN, J. Int. Meteor. Organ., 29, 134
Jenniskens, P., & Vaubaillon, J. 2008, Earth Moon Planets, 102, 157
Jopek, T., Rudawska, R., & Pretka-Ziomek, H. 2006, MNRAS, 371, 1367
Kareta, T., Noonan, J. W., Harris, W. M., & Springmann, A. 2023, PSJ, 4, 85
Koten, P., Borovička, J., Spurný, P., & Štork, R. 2007, A&A, 466, 729
Koten, P., Shrbený, L., Spurný, P., et al. 2023, A&A, 675, A70
Maslov, M. P., & Muzyko, E. I. 2017, Earth Moon Planets, 119, 85
Moorhead, A. V., Clements, T., & Vida, D. 2021, MNRAS, 508, 326
Moser, D. E., & Cooke, W. J. 2004, Earth Moon Planets, 95, 141
Moser, D. E., & Cooke, W. J. 2008, Earth Moon Planets, 102, 285
Moulane, Y., Jehin, E., Manfroid, J., et al. 2023, A&A, 670, A159
Rendtel, J. 2004, in 22nd IMC, Bollmannsruh, Germany, Proc. Int. Meteor Conf., 2003, 114
Rickman, H., & Jorda, L. 1998, Adv. Space Res., 21, 1491
Schulz, R., & Schwehm, G. 1999, in Composition and Origin of Cometary Materials: Proceedings of an ISSI (Bern, Switzerland: Springer), 321
Vaubaillon, J., Lamy, P., & Jorda, L. 2004, Earth Moon Planets, 95, 75
Vaubaillon, J., Colas, F., & Jorda, L. 2005a, A&A, 439, 751
Vaubaillon, J., Colas, F., & Jorda, L. 2005b, A&A, 439, 761
Vaubaillon, J., Ye, Q.-Z., Egal, A., Sato, M., & Moser, D. 2023, A&A, 680, L10
Vida, D., Brown, P. G., & Campbell-Brown, M. 2018, MNRAS, 479, 4307
Vida, D., Campbell-Brown, M., Brown, P. G., Egal, A., & Mazur, M. J. 2020a, A&A, 635, A153
Vida, D., Gural, P. S., Brown, P. G., Campbell-Brown, M., & Wiegert, P. 2020b, MNRAS, 491, 2688
Vida, D., Šegon, D., Gural, P. S., et al. 2021, MNRAS, 506, 5046
Vida, D., Blaauw Erskine, R. C., Brown, P. G., et al. 2022, MNRAS, 515, 2322
Watanabe, J.-I., Sato, M., & Kasuga, T. 2005, PASJ, 57, L45
Weryk, R. J., & Brown, P. G. 2013, Planet. Space Sci., 81, 32
Ye, Q., & Jenniskens, P. 2022, arXiv e-prints [arXiv:2209.10654]
Ye, Q.-Z., Hui, M.-T., Brown, P. G., et al. 2016, Icarus, 264, 48

Appendix A: Meteor trajectories and orbits

Table A.1. Trajectory and orbit parameters of the observed meteors by the Global Meteor Network.

Time (UTC)	$\lambda_\odot$ (deg)	α_g (deg)	δ_g (deg)	V_g (km/s)	a (au)	e	i (deg)	q (au)	Ω (deg)	ω (deg)	π (deg)	h_B (km)	h_E (km)	$h_{\rm peak}$ (km)	$M_{\rm peak}$ (mag)	K_B
09:41:46.307	259.760586	7.84	-38.62	10.392	3.140	0.6864	9.439	0.9846310	79.768747	0.30	80.07	90.218	76.819	84.199	+0.21	6.94
		0.32	0.18	0.074	0.070	0.0069	0.038	0.0000000		0.14	0.14	0.050	0.040			
10:30:52.915	259.795268	7.16	-38.43	9.900	2.832	0.6523	8.991	0.9846280	79.802844	0.08	79.88	89.853	78.091	81.758	+0.46	6.97
		0.21	0.20	0.061	0.032	0.0040	0.079	0.0000000		0.10	0.10	0.030	0.020			
10:45:53.244	259.805864	7.76	-39.13	10.579	3.254	0.6974	9.668	0.9846250	79.813104	0.07	79.88	89.906	81.326	86.231	+1.65	7.00
		1.77	1.10	0.684	0.901	0.0542	0.447	0.0002000		1.08	1.08	0.160	0.170			
10:55:57.111	259.812971	5.82	-40.22	10.359	3.060	0.6782	9.558	0.9845520	79.819086	358.87	78.69	89.323	77.529	81.388	-0.07	7.03
		0.63	0.77	0.085	0.046	0.0049	0.187	0.0000000		0.44	0.44	0.060	0.060			
11:05:57.961	259.820043	8.29	-39.09	10.100	2.896	0.6601	9.365	0.9846180	79.826519	0.34	80.17	88.731	77.457	81.778	-0.45	7.07
		0.59	0.44	0.140	0.131	0.0130	0.065	0.0000000		0.33	0.33	0.050	0.030			
12:00:04.960	259.858260	6.56	-38.65	9.861	2.808	0.6494	8.955	0.9846150	79.864074	359.71	79.58	91.385	77.007	87.773	+1.77	6.86
		0.42	0.14	0.134	0.067	0.0084	0.152	0.0000000		0.14	0.14	0.070	0.060			
12:46:23.484	259.890963	6.58	-39.45	9.782	2.722	0.6383	9.057	0.9846060	79.902111	359.45	79.35	92.840	77.232	83.906	+0.20	6.75
		0.19	0.33	0.095	0.070	0.0088	0.021	0.0000000		0.18	0.18	0.070	0.030			
12:57:12.681	259.898605	6.79	-39.27	9.831	2.755	0.6426	9.076	0.9846140	79.909016	359.59	79.50	90.072	72.864	81.493	-0.44	6.94
		0.33	0.17	0.057	0.043	0.0058	0.016	0.0000000		0.13	0.13	0.020	0.020			
13:01:31.386	259.901649	6.27	-37.72	9.848	2.853	0.6549	8.739	0.9846130	79.907307	359.85	79.76	89.511	81.264	85.819	+0.95	7.03
		0.56	0.99	0.158	0.052	0.0061	0.336	0.0000000		0.24	0.24	0.070	0.060			
13:07:48.998	259.906093	6.26	-37.86	9.996	2.942	0.6653	8.868	0.9846170	79.916954	359.78	79.70	89.483	77.391	83.160	+1.26	7.00
		0.27	1.65	0.440	0.344	0.0435	0.033	0.0000000		0.42	0.42	0.130	0.130			
13:14:46.735	259.911011	6.89	-39.91	9.730	2.666	0.6307	9.134	0.9846020	79.920482	359.43	79.35	88.251	79.740	83.293	+1.11	7.06
		0.24	0.41	0.097	0.033	0.0048	0.154	0.0000000		0.14	0.14	0.020	0.010			
13:21:43.108	259.915911	7.09	-39.44	9.903	2.783	0.6462	9.186	0.9846120	79.925115	359.66	79.58	92.288	74.862	81.079	-0.43	6.78
		0.19	0.18	0.024	0.003	0.0003	0.066	0.0000000		0.06	0.06	0.020	0.020			
13:22:48.440	259.916680	6.04	-38.38	9.692	2.732	0.6396	8.740	0.9846030	79.921885	359.55	79.47	91.239	80.946	85.689	+0.92	6.89
		0.25	0.15	0.015	0.012	0.0016	0.045	0.0000000		0.11	0.11	0.030	0.030			
13:30:12.540	259.921907	10.80	-38.57	10.269	2.972	0.6688	9.610	0.9844630	79.926941	1.57	81.49	89.407	82.104	84.754	+2.40	7.06
		2.30	0.28	0.182	0.060	0.0074	0.366	0.0001000		0.95	0.95	0.150	0.120			
13:44:07.285	259.931732	9.26	-37.94	10.364	3.122	0.6847	9.411	0.9845450	79.940239	1.07	81.01	90.921	78.231	84.105	+0.49	6.90
		0.65	1.74	0.466	0.186	0.0245	0.697	0.0001000		0.32	0.32	0.190	0.060			
14:39:26.951	259.970805	6.97	-39.04	10.235	3.020	0.6739	9.335	0.9846000	79.978607	359.68	79.66	90.153	79.277	86.483	+0.80	6.97
		0.20	0.15	0.034	0.011	0.0012	0.068	0.0000000		0.07	0.07	0.020	0.010			
15:02:38.789	259.987187	6.28	-39.95	9.931	2.789	0.6470	9.236	0.9846210	80.002258	359.10	79.10	90.100	71.945	76.310	-0.26	7.17
		0.12	0.09	0.026	0.018	0.0023	0.011	0.0000000		0.08	0.08	0.070	0.040			
15:24:13.360	260.002425	6.26	-37.78	10.088	3.009	0.6728	8.915	0.9845980	80.009246	359.75	79.76	88.584	80.556	85.417	+0.99	7.09
		0.72	0.75	0.072	0.016	0.0017	0.258	0.0000000		0.18	0.18	0.040	0.050			
15:32:00.210	260.007921	9.66	-38.34	9.938	2.804	0.6489	9.221	0.9845250	80.015119	1.11	81.12	88.757	78.596	83.334	+0.88	7.07
		1.06	0.29	0.026	0.010	0.0013	0.064	0.0000000		0.55	0.55	0.040	0.070			
16:06:14.321	260.032097	7.38	-39.37	10.243	2.996	0.6714	9.442	0.9846270	80.038368	359.73	79.77	91.896	83.424	88.004	+1.24	6.96
		0.40	0.30	0.121	0.077	0.0085	0.109	0.0000000		0.27	0.27	0.050	0.040			
16:33:46.541	260.051545	6.75	-39.84	10.218	2.965	0.6679	9.464	0.9845640	80.057597	359.29	79.35	90.695	76.727	85.900	+0.13	6.94
		0.67	0.08	0.047	0.041	0.0049	0.022	0.0000000		0.32	0.32	0.040	0.080			
16:55:42.027	260.067029	8.74	-38.89	10.120	2.909	0.6616	9.381	0.9845780	80.073024	0.47	80.55	90.502	81.624	84.233	+1.90	6.95
		1.00	0.20	0.031	0.011	0.0012	0.080	0.0000000		0.50	0.50	0.070	0.060			
17:11:49.569	260.078417	6.08	-38.88	9.610	2.663	0.6302	8.780	0.9845680	80.084380	359.33	79.42	90.613	82.306	85.386	+1.35	6.92
		0.72	0.28	0.066	0.033	0.0044	0.071	0.0000000		0.39	0.39	0.080	0.010			

All meteors were observed on December 12. Standard deviations of individual parameters are given in alternating rows. $\lambda_\odot$ is the solar longitude, α_g and δ_g are geocentric right ascension and declination in J2000, V_g is the geocentric velocity, a is the semi-major axis, e is the eccentricity, i is the inclination, q is the perihelion distance, Ω is the ascending node, ω is the argument of perihelion, π is the longitude of perihelion, h_B is the meteor being height, h_E is the end height, $h_{\rm peak}$ is the height of peak magnitude, $M_{\rm peak}$ is the peak magnitude, and K_B is the Ceplecha (1958) parameter.

Table A.2. Flux measurements by the GMN.

$\lambda_\odot$ (deg)	Flux(+6.5) (met / 1000 km^2 h)	Flux(+5.42) (met / 1000 km^2 h)	ZHR (met/h)	Meteor Count	TAP (1000 km^2 h)	Meteor LM (mag)	Radiant elev. (deg)	Radiant dist. (deg)	Ang vel. (deg/s)
259.7351911	$0.125^{+0.106}_{-0.065}$	$0.038^{+0.032}_{-0.020}$	$0.138^{+0.115}_{-0.072}$	10	79.760	5.36	52.58	61.34	6.08
259.8190395	$0.138^{+0.117}_{-0.072}$	$0.042^{+0.035}_{-0.022}$	$0.152^{+0.127}_{-0.079}$	10	72.255	5.45	43.28	64.32	6.37
259.8635306	$0.163^{+0.116}_{-0.076}$	$0.050^{+0.035}_{-0.024}$	$0.179^{+0.127}_{-0.084}$	13	79.795	5.46	53.29	60.99	6.03
259.9063104	$0.360^{+0.139}_{-0.108}$	$0.110^{+0.042}_{-0.033}$	$0.395^{+0.152}_{-0.118}$	36	99.887	5.53	56.61	58.49	5.87
259.9473790	$0.275^{+0.149}_{-0.107}$	$0.084^{+0.045}_{-0.033}$	$0.301^{+0.164}_{-0.117}$	20	72.807	5.46	52.77	61.90	5.95
259.9884477	$0.588^{+0.243}_{-0.186}$	$0.179^{+0.074}_{-0.057}$	$0.646^{+0.265}_{-0.204}$	32	54.381	5.41	46.60	65.48	6.10
260.0312275	$0.377^{+0.235}_{-0.162}$	$0.115^{+0.071}_{-0.049}$	$0.413^{+0.258}_{-0.177}$	16	42.488	5.41	43.32	66.76	6.10
260.0740073	$0.435^{+0.295}_{-0.197}$	$0.132^{+0.090}_{-0.060}$	$0.477^{+0.324}_{-0.216}$	14	32.179	5.38	35.02	72.36	6.24
260.1321879	$0.234^{+0.197}_{-0.122}$	$0.071^{+0.060}_{-0.037}$	$0.257^{+0.216}_{-0.134}$	10	42.696	5.33	26.98	78.32	6.23
260.3187080	$0.113^{+0.090}_{-0.056}$	$0.034^{+0.028}_{-0.017}$	$0.124^{+0.098}_{-0.062}$	11	97.173	5.31	34.52	71.62	6.71

$\lambda_\odot$ is the time-area product (TAP) weighted solar longitude of the bin. The two flux columns are fluxes at the standard magnitude of +6.5 and the measured mean magnitude of +5.42. Meteor LM is the mean TAP-weighted apparent meteor limiting magnitude, followed by the mean radiant parameters weighted in the same way.

Appendix B: Additional figures

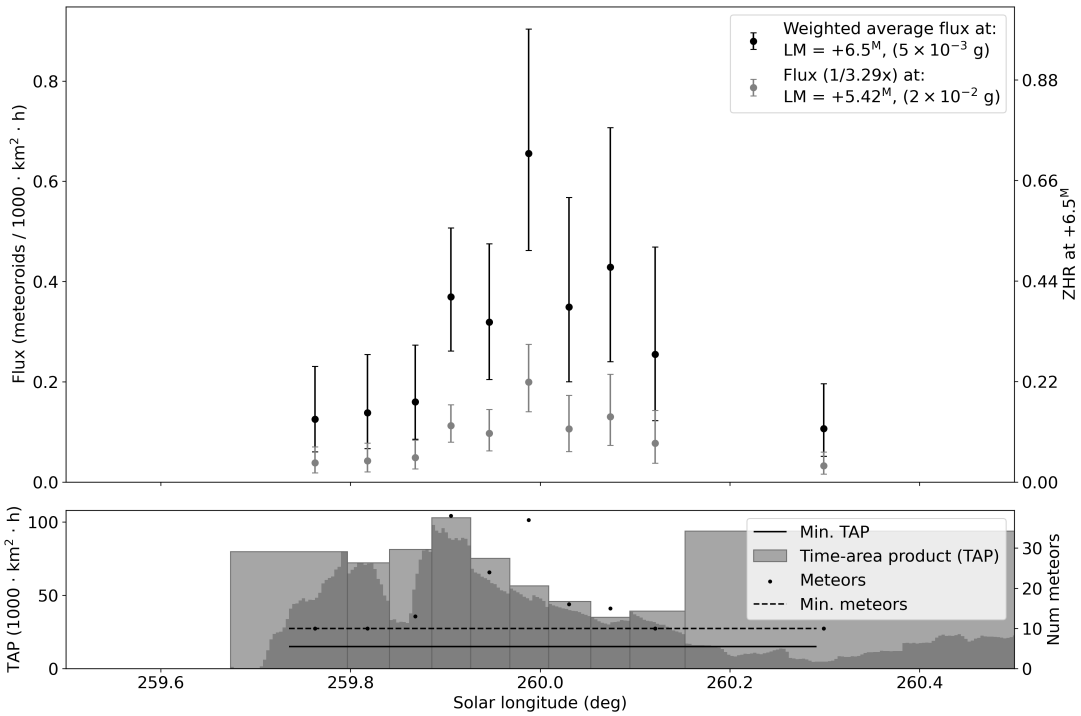

Fig. B.1. Flux profile of the λ-Sculpturids. The top inset shows the flux at two different limiting magnitudes: black markers for the standard +6.5 and gray markers for the observed mean of +5.42. The bottom inset shows the observed time-area product (TAP) and the observed number of meteors, together with the thresholds set on both. The dark gray shading inside individual TAP bins shows the distribution of TAP inside each bin, revealing any potential gaps in coverage.

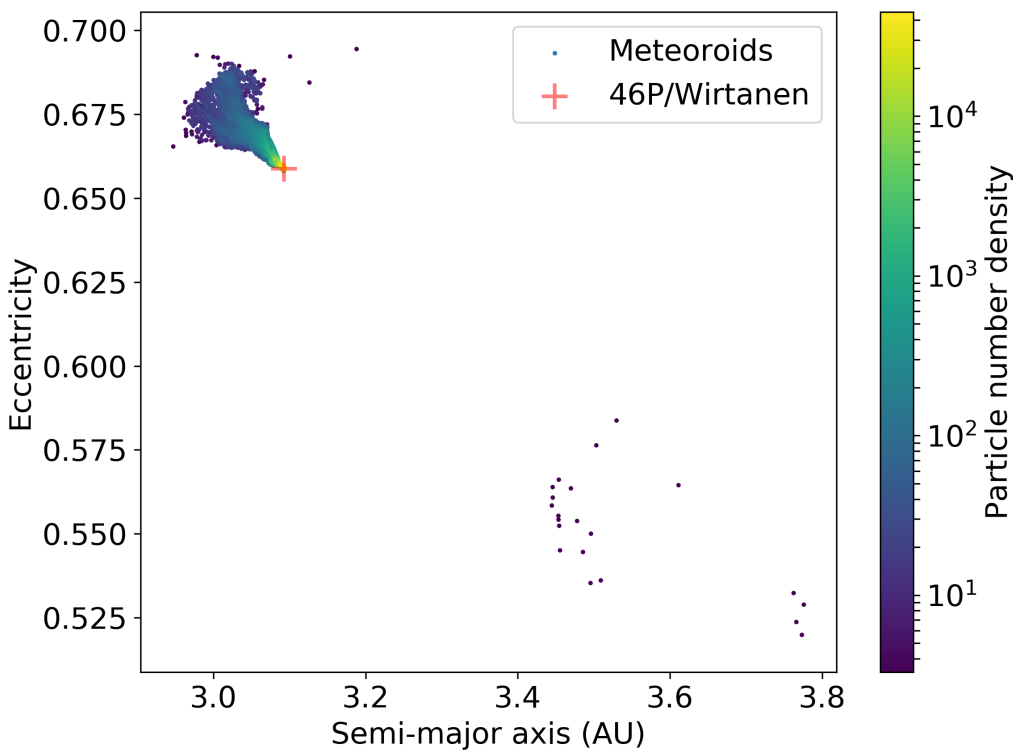

Fig. B.2. Orbits of simulated particles encountering the Earth in 2023, ejected in 1974 (JV model). Particles are coloured by the relative number density. The red marker is the orbit of 46P/Wirtanen. The close encounter with Jupiter in 1984 caused the so-called reversal process, eventually making the meteoroids lead the parent.

Appendix C: Extended acknowledgements

The authors thank all Global Meteor Network camera operators and contributors:
Adam Mullins, Aden Walker, Adrian Bigland, Adriana Roggemans, Alain Marin, Alan Beech, Alan Maunder, Alan Pevec, Alan Pickwick, Alan Decamps, Alan Cowie, Aled Powell, Alejandro Barriuso, Aleksandar Merlak, Alex Bell, Alex Haislip, Alex Hodge, Alex Jeffery, Alex Kichev, Alex McConahay, Alex Pratt, Alex Roig, Alex Aitov, Alexander Wiedekind-Klein, Alexandre Alves, Alfredo Dal' Ava Júnior, Amy Barron, Anatoly Ijon, Andre Rousseau, Andre Bruton, Andrea Storani, Andrei Marukhno, Andres Fernandez, Andrew Campbell-Laing, Andrew Challis, Andrew Cooper, Andrew Fiamingo, Andrew Heath, Andrew Moyle, Andrew Washington, Andy Stott, Andy Sapir, Ange Fox, Angel Sierra, Angélica López Olmos, Ansgar Schmidt, Anthony Hopkinson, Anthony Pitt, Anthony Kesterton, Anton Macan, Anton Yanishevskiy, Anzhari Purnomo, Arie Blumenzweig, Arie Verveer, Arnaud Leroy, Attila Nemes, Barry Findley, Bart Dessoy, Bela Szomi Kralj, Bernard Côté, Bernard Hagen, Bev M. Ewen-Smith, Bill Cooke, Bill Wallace, Bill Witte, Bill Carr, Bob Evans, Bob Greschke, Bob Hufnagel, Bob Marshall, Bob Massey, Bob Zarnke, Bob Guzik, Brenda Goodwill, Brendan Cooney, Brian Chapman, Brian Murphy, Brian Rowe, Brian Hochgurtel, Wyatt Hochgurtel, Brian Mitchell, Bruno Bonicontro, Callum Potter, Carl Elkins, Carl Mustoe, Carl Panter, Charles Thody, Charlie McCormack, Chris Baddiley, Chris Blake, Chris Dakin, Chris George, Chris James, Chris Ramsay, Chris Reichelt, Chris Chad, Chris O'Neill, Chris White, Christian Wanlin, Christine Ord, Christof Zink, Christophe Demeautis, Christopher Coomber, Christopher Curtis, Christopher Tofts, Christopher Brooks, Chuck Goldsmith, Chuck Pullen, Ciaran Tangney, Claude Boivin, Claude Surprenant, Clive Sanders, Colin Graham, Colin Marshall, Colin Nichols, Con Stoitsis, Creina Beaman, Daknam Al-Ahmadi, Damien Lemay, Damien McNamara, Damir Matković, Damir Šegon, Damjan Nemarnik, Dan Klinglesmith, Dan Pye, Daniel Duarte, Daniel J. Grinkevich, Daniela Cardozo Mourão, Danijel Reponj, Danko Kočiš, Dario Zubović, Dave Jones, Dave Mowbray, Dave Newbury, Dave Smith, David Akerman, David Attreed, David Bailey, David Brash, David Castledine, David Hatton, David Leurquin, David Price, David Rankin, David Robinson, David Rollinson, David Strawford, David Taylor, David Rogers, David Banes, David Johnston, David Rees, Dean Moore, Denis Bergeron, Denis St-Gelais, Dennis Behan, Derek Poulton, Didier Walliang, Dimitris Georgoulas, Dino Čaljkušić, Dmitrii Rychkov, Dominique Guiot, Don Anderson, Don Hladiuk, Dorian Božičević, Dougal Matthews, Douglas Sloane, Douglas Stone, Dustin Rego, Dylan O'Donnell, Ed Breuer, Ed Harman, Edd Stone, Edgar Mendes Merizio, Edison José Felipe Pérezgómez Álvarez, Edson Valencia Morales, Eduardo Fernandez Del Peloso, Edward Cooper, Ehud Behar, Eleanor Mayers, Enrico Pettarin, Enrique Arce, Enrique Chávez Garcilazo, Eric Lopez, Eric Toops, Erwin van Ballegoij, Erwin Harkink, Eugene Potapov, Ewan Richardson, Fabricio Borges, Fernando Dall'Igna, Fernando Jordan, Fernando Requena, Filip Matković, Filip Mezak, Filip Parag, Fiona Cole, Florent Benoit, Francis Rowsell, François Simard, Frank Lyter, Frantisek Bilek, Gabor Sule, Gaétan Laflamme, Gareth Brown, Gareth Lloyd, Gareth Oakey, Garry Dymond, Gary Parker, Gary Eason, Gavin Martin, Gene Mroz, Geoff Scott, Georges Attard, Georgi Momchilov, Germano Soru, Gilton Cavallini, Gordon Hudson, Graeme Hanigan, Graham Stevens, Graham Winstanley, Graham Henstridge, Greg Michael, Gustav Frisholm, Gustavo Silveira B. Carvalho, Guy Létourneau, Guy Williamson, Guy Lesser, Hamish Barker, Hamish McKinnon, Haris Jeffrey, Harri Kiiskinen, Hartmut Leiting, Heather Petelo, Heriton Rocha, Hervé Lamy, Herve Roche, Holger Pedersen, Horst Meyerdierks, Howard Edin, Hugo González, Iain Drea, Ian Enting Graham, Ian Lauwerys, Ian Parker, Ian Pass, Ian A. Smith, Ian Williams, Ian Hepworth, Ian Collins, Igor Duchaj, Igor Henrique, Igor Macuka, Igor Pavletić, Ilya Jankowsky, Ioannis Kedros, Ivan Gašparić, Ivan Sardelić, Ivica Ćiković, Ivica Skokić, Ivo Dijan, Ivo Silvestri, Jack Barrett, Jacques Masson, Jacques Walliang, Jacqui Thompson, James Davenport, James Farrar, James Scott, James Stanley, James Dawson, Jamie Allen, Jamie Cooper, Jamie McCulloch, Jamie Olver, Jamie Shepherd, Jan Hykel, Jan Wisniewski, Janis Russell, Janusz Powazki, Jason Burns, Jason Charles, Jason Gill, Jason van Hattum, Jason Sanders, Javor Kac, Jay Shaffer, Jean Francois Larouche, Jean Vallieres, Jean Brunet, Jean-Baptiste Kikwaya, Jean-Louis Naudin, Jean-Marie Jacquart, Jean-Paul Dumoulin, Jean-Philippe Barrilliot, Jeff Holmes, Jeff Huddle, Jeff Wood, Jeff Devries, Jeffrey Legg, Jeremy Taylor, Jesse Stayte, Jesse Lard, Jessica Richards, Jim Blackhurst, Jim Cheetham, Jim Critchley, Jim Fordice, Jim Gilbert, Jim Rowe, Jim Seargeant, Jochen Vollsted, Jocimar Justino, John W. Briggs, John Drummond, John Hale, John Kmetz, John Maclean, John Savage, John Thurmond, John Tuckett, John Waller, John Wildridge, John Bailey, Jon Bursey, Jonathan Alexis Valdez Aguilar, Jonathan Eames, Jonathan Mackey, Jonathan Whiting, Jonathan Wyatt, Jonathon Kambulow, Jorge Augusto Acosta Bermúdez, Jorge Oliveira, Jose Carballada, Jose Galindo Lopez, José María García, José-Luis Martín, Josip Belas, Josip Krpan, Jost Jahn, Juan Luis Muñoz, Jure Zakrajáek, Jürgen Dörr, Jürgen Ketterer, Justin Zani, Karen Smith, Kath Johnston, Kees Habraken, Keith Maslin, Keith Biggin, Ken Jamrogowicz, Ken Lawson, Ken Gledhill, Kevin Gibbs-Wragge, Kevin Morgan, Klaas Jobse, Korado Korlević, Kyle Francis, Lachlan Gilbert, Larry Groom, Laurent Brunetto, Laurie Stanton, Lawrence Saville, Lee Hill, Len North, Leslie Kaye, Lev Pustil'Nik, Lexie Wallace, Lisa Holstein, Llewellyn Cupido, Lorna McCalman, Louw Ferreira, Lovro Pavletić, Lubomir Moravek, Luc Turbide, Lucia Dowling, Luciano Miguel Diniz, Ludger Börgerding, Luis Fabiano Fetter, Maciej Reszelsk, Magda Wisniewska, Manel Colldecarrera, Marc Corretgé Gilart, Marcel Berger, Marcelo Domingues, Marcelo Zurita, Marcio Malacarne, Marco Verstraaten, Margareta Gumilar, Marián Harnádek, Mariusz Adamczyk, Mark Fairfax, Mark Gatehouse, Mark Haworth, Mark McIntyre, Mark Phillips, Mark Robbins, Mark Spink, Mark Suhovecky, Mark Williams, Mark Ward, Marko Áegon, Marthinus Roos, Martin Breukers, Martin Richmond-Hardy, Martin Robinson, Martin Walker, Martin Woodward, Martin Connors, Martyn Andrews, Mason McCormack, Mat Allan, Matej Mihelčić, Matt Cheselka, Matthew Howarth, Megan Gialluca, Mia Boothroyd, Michael Cook, Michael Mazur, Michael O'Connell, Michael Krocil, MichałWarchoł, Michel Saint-Laurent, Miguel Diaz Angel, Miguel Preciado, Mike Breimann, Mike Hutchings, Mike Read, Mike Shaw, Mike Ball, Milan Kalina, Minesh Patel, Mirjana Malarić, Muhammad Luqmanul Hakim Muharam, Murray Forbes, Murray Singleton, Murray Thompson, Myron Valenta, Nawaz Mahomed, Ned Smith, Nedeljko Mandić, Neil Graham, Neil Papworth, Neil Waters, Neil Petersen, Nelson Moreira, Neville Vann, Nial Bruce, Nicholas Hill, Nicholas Ruffier, Nick Howarth, Nick James, Nick Moskovitz, Nick Norman, Nick Primavesi, Nick Quinn, Nick Russel, Nicola Masseroni, Nigel

Bubb, Nigel Evans, Nigel Owen, Nigel Harris, Nikola Gotovac, Nikolay Gusev, Nikos Sioulas, Noah Simmonds, Ollie Eisman, Pablo Canedo, Paraksh Vankawala, Pat Devine, Patrick Franks, Patrick Poitevin, Patrick Geoffroy, Patrik Kukić, Paul Cox, Paul Dickinson, Paul Haworth, Paul Heelis, Paul Kavanagh, Paul Ludick, Paul Prouse, Paul Pugh, Paul Roche, Paul Roggemans, Paul Stewart, Paul Huges, Pedro Augusto Hay Day, Penko Yordanov, Pete Graham, Pete Lynch, Peter G. Brown, Peter Campbell-Burns, Peter Davis, Peter Eschman, Peter Gural, Peter Hallett, Peter Jaquiery, Peter Kent, Peter Lee, Peter McKellar, Peter Meadows, Peter Stewart, Peter Triffitt, Peter Leigh, Petö Zsolt, Phil James, Philip Gladstone, Philip Norton, Philippe Schaak, Phillip Wilhelm Maximilian Grammerstorf, Pierre Gamache, Pierre de Ponthière, Pierre-Michael Micaletti, Pierre-Yves Pechart, Pieter Dijkema, Predrag Vukovic, Przemek Nagański, Radim Stano, Rajko Sušanj, Raju Aryal, Raoul van Eijndhoven, Raul Truta, Reinhard Kühn, Remi Lacasse, Renato Cássio Poltronieri, René Tardif, Richard Abraham, Richard Bassom, Richard Croy, Richard Davis, Richard Fleet, Richard Hayler, Richard Johnston, Richard Kacerek, Richard Payne, Richard Stevenson, Richard Severn, Rick Fischer, Rick Hewett, Rick James, Ricky Bassom, Rob Agar, Rob de Corday Long, Rob Saunders, Rob Smeenk, Robert Longbottom, Robert McCoy, Robert Saint-Jean, Robert D. Steele, Robert Veronneau, Robert Peledie, Robin Boivin, Robin Earl, Robin Rowe, Roel Gloudemans, Roger Banks, Roger Morin, Roland Idaczyk, Rolf Carstens, Romulo Jose, Ron James Jr, Roslina Hussain, Russell Jackson, Ryan Frazer, Ryan Harper, Salvador Aguirre, Sam Green, Sam Hemmelgarn, Sarah Tonorio, Scott Kaufmann, Sebastian Klier, Seppe Canonaco, Seraphin Feller, Serge Bergeron, Sergio Mazzi, Sevo Nikolov, Simon Cooke-Willis, Simon Holbeche, Simon Maidment, Simon McMillan, Simon Minnican, Simon Parsons, Simon Saunders, Simon Fidler, Sofia Ulrich, Srivishal Sudharsan, Stacey Downton, Stan Nelson, Stanislav Korotkiy, Stanislav Tkachenko, Stef Vancampenhout, Stefan Frei, Stephane Zanoni, Stephen Grimes, Stephen Nattrass, Steve Berry, Steve Bosley, Steve Carter, Steve Dearden, Steve Homer, Steve Kaufman, Steve Lamb, Steve Rau, Steve Tonkin, Steve Trone, Steve Welch, Steven Shanks, Steven Tilley, Stewart Doyle, Stuart Brett, Stuart Land, Stuart McAndrew, Sylvain Cadieux, Tammo Jan Dijkema, Terry Pundiak, Terry Richardson, Terry Simmich, Terry Young, Thiago Paes, Thomas Blog, Thomas Schmiereck, Thomas Stevenson, Tihomir Jakopčić, Tim Burgess, Tim Claydon, Tim Cooper, Tim Gloudemans, Tim Havens, Tim Polfliet, Tim Frye, Tioga Gulon, Tobias Westphal, Tom Warner, Tommy McEwan, Tommy B. Nielsen, Torcuill Torrance, Tosh White, Tracey Snelus, Trevor Clifton, Ubiratan Borges, Urs Wirthmueller, Uwe Glässner, Vasilii Savtchenko, Ventsislav Bodakov, Victor Acciari, Viktor Toth, Vincent McDermott, Vladimir Jovanović, Waily Harim, Warley Souza, Washington Oliveira, Wenceslao Trujillo, William Perkin, William Schauff, William Stewart, William Harvey, William Hernandez, Wullie Mitchell, Yakov Tchenak, Yfore Scott, Yohsuke Akamatsu, Yong-Ik Byun, Yozhi Nasvadi, Yuri Stepanychev, Zach Steele, Zané Smit, Zbigniew Krzeminski, Željko Andreić, Zhuoyang Chen, Zoran Dragić, Zoran Knez, Zoran Novak, Asociación de Astronomía de Marina Alta, Costa Blanca Astronomical Society, Perth Observatory Volunteer Group, Royal Astronomical Society of Canada Calgary Centre.